



## Investigation of post-annealing treatment effect on film properties of sputter-deposited BiVO<sub>4</sub> nanoporous photocatalyst

Siavash Bakhtiarnia<sup>1,2</sup>, Saeed Sheibani<sup>\*1</sup>, Alain Billard<sup>2</sup>, Eric Aubry<sup>2</sup>, Hui Sun<sup>3</sup>, Mohammad Arab Pour Yazdi<sup>2</sup>

<sup>1</sup>School of Metallurgy and Materials Engineering, College of Engineering, University of Tehran, Tehran, Iran;

<sup>2</sup>Institut FEMTO-ST, UMR 6174, CNRS, Univ. Bourgogne Franche-Comté, 15B, Avenue des Montboucons, 25030 Besançon, France;

<sup>3</sup>School of Space Science and Physics, Shandong University, Weihai 264209, China.

Received: 23 November 2021; Accepted: 7 January 2022

\*Corresponding author email: [ssheibani@ut.ac.ir](mailto:ssheibani@ut.ac.ir)

### ABSTRACT

Nanoporous BiVO<sub>4</sub> thin films were deposited on fused silica substrate using reactive magnetron sputtering. The effect of annealing temperature on the microstructure, morphology and optical properties was evaluated. The samples were characterized by X-ray diffraction (XRD), field-emission scanning electron microscopy (FESEM), energy dispersive spectroscopy (EDS), ultraviolet-visible spectroscopy (UV-Vis) and X-ray photoelectron spectroscopy (XPS). XPS demonstrated the Bi<sup>+3</sup> and V<sup>+5</sup> oxidation states, as well as the adsorbed and lattice oxygen on the film surface. The as-deposited films proved to be amorphous by the XRD results, while the pure monoclinic scheelite BiVO<sub>4</sub> crystal structure was obtained after a post-annealing treatment at 300 and 450 °C. FESEM images displayed a uniform surface with no grain boundaries for the as-deposited film, whereas nanopores with an average diameter of 20-40 nm were observable in the film annealed at 450 °C as opposed to the film annealed at 300 °C with a dense and cracked surface. The association of nanoporosity with the efficiency of visible-light absorption was demonstrated by the UV-Vis spectrophotometry results with the narrowest bandgap (2.5 eV) concerning the film annealed at 450 °C. The photocatalytic experiment under visible light showed an 80 % photodegradation of Rhodamine-B solution after 7 h, and the recycling experiment proved the stability of the thin films after three cycles. These results show the great potential of BiVO<sub>4</sub> thin films deposited by reactive magnetron sputtering in photocatalytic wastewater treatment applications.

**Keywords:** Sputtering; BiVO<sub>4</sub>; Thin Film; Photocatalysis; Spectroscopy.

### 1. Introduction

Photocatalysis has been extensively studied in the past decades for various applications e.g. hydrogen production [1], air purification [2] and water treatment [3,4]. Semiconductors have been proven to be effective in the photodegradation of organic pollutants such as organic dyes of the textile industry [5], bacteria inactivation [6], antibiotics in hospital wastewater [7] and industrial phenolic compounds [8]. TiO<sub>2</sub> was at the center of the attention due to high stability, high photoactivity

and inexpensive production [9,10], though, some drawbacks including the lack of photoactivity in the visible light as a result of having a wide bandgap (> 3 eV), revealed the absolute need to develop other semiconductors [11].

Monoclinic BiVO<sub>4</sub> attracted lots of attention owing to its interesting properties like low bandgap (~2.4 eV), high photoactivity under visible light, stability and facile production [12]. Numerous research could be found in the literature, synthesizing BiVO<sub>4</sub> through chemical methods

such as hydrothermal [13,14], sol-gel [15] and co-precipitation [16], while the physical methods like sputtering received less attention. Although most researchers that studied the photocatalytic properties of  $\text{BiVO}_4$  utilized the powder form due to some advantages like high specific surface and facile production [17], powder form photocatalysts bring certain downsides like recyclability resulting in a huge operational cost to separate the powder from water. Some solutions have been proposed like core-shell structures for magnetic separation [18] which also comes with challenges in the synthesis process. Preparing photocatalysts in thin-film form is an excellent solution for solving the reusability and recyclability issues to make the photocatalysis process more economically feasible. Reactive magnetron sputtering with many advantages like being cost-efficient, mass-producible, uniform products and versatility [19] is ideal to deposit thin films for photocatalysis applications, though despite the corresponding upsides, few researchers employed this technique to produce  $\text{BiVO}_4$  thin films. Moreover, there are some drawbacks to  $\text{BiVO}_4$  photocatalysts limiting its performance such as low carrier mobility, high recombination rate and low specific surface [20]. These limitations need to be addressed in order to be able to prepare the fully functional photocatalyst with the optimum performance. Researchers proposed different techniques to remove the mentioned barriers and enhance photocatalytic activity. Our team prepared Ag-incorporated  $\text{BiVO}_4$  thin films by reactive magnetron sputtering [21], and the results with 99 % RhB photodegradation showed significant enhancement over pristine  $\text{BiVO}_4$  due to  $\text{Ag}_4\text{V}_2\text{O}_7/\text{BiVO}_4$  heterostructure reducing recombination rate, as well as the plasmonic effect of Ag nanoparticles enhancing the light absorption. Ullah et al. [22], using the density functional theory method proposed that Se-doped  $\text{BiVO}_4$  with oxygen vacancies enhances the carriers' mobility, as well as optimizes the bandgap and band edge potentials thus improving photocatalytic activity. Creating nanoporous morphology

could be considered as another suitable solution that effectively enhances photocatalytic activity through increasing the photoreaction surface and active sites, as well as photon entrapment and light absorption [23]. It could also solve the low specific surface problem inherent to thin films compared to powder photocatalysts. However, this solution did not receive proper attention from the researchers.

This research aims to investigate the influence of the post-annealing treatment on the nanoporous morphology of the sputter-deposited  $\text{BiVO}_4$  thin films since the effect of the annealing temperature has never been studied on the  $\text{BiVO}_4$  thin films prepared by reactive magnetron sputtering. Further, to assess the influence of the post-annealing treatment and nanoporosity of the thin films annealed at different temperatures comparatively on the film properties, e.g., crystal structure, morphology, porosity, optical properties and photocatalytic activity. The evaluation of the stability of the thin films in the acidic pH conditions could also prove the value of the thin films in terms of recyclability and reusability for industrial photocatalytic water treatment applications.

## 2. Experimental procedure

### 2.1. Film deposition

Bi and V metallic targets were used to prepare  $\text{BiVO}_4$  thin films on fused silica substrate ( $50 \times 3$  mm) in argon and oxygen atmosphere at room temperature. The synthesis parameters are provided in Table 1.

A dual pulsed direct current (DC) generator was utilized to provide the discharge power. The substrates were fully cleaned by water and soap before deposition. The discharge power was adjusted properly to reach a Bi:V atomic ratio of 1 to implement a stoichiometric composition. The oxygen flow in the chamber provided the necessary reactive condition to produce the oxide film.

### 2.2. Characterizations

The crystal structure of the films was characterized using the X-ray diffraction (XRD)

Table 1-  $\text{BiVO}_4$  thin films sputtering deposition parameters

Ar flow rate (sccm)	200	Targets	Bi	V
O <sub>2</sub> flow rate (sccm)	20	Intensity (A)	0.07	0.64
Total pressure (Pa)	4.5	Power (W)	9	235
Runtime (h)	3	Frequency (kHz)	70	50
Drawing distance (mm)	60	T <sub>off</sub> (μs)	4	4

method (BRUKER AXS) equipped with a cobalt X-ray tube ( $\lambda_{\text{K}\alpha 1} = 0.178897 \text{ nm}$ ). The average of crystallite size of the samples was also calculated by the Scherrer equation using the XRD data. X-ray photoelectron spectroscopy (XPS, Thermo ESCALAB 250Xi) was used to evaluate the chemical state of the film surface, as well as the elements' oxidation states. The XPS spectra were charge corrected using C 1s at the standard value of 284.8 eV [24]. The optical transmittance and reflectance of the films were measured by a UV-Vis spectrophotometer (UV-3600, Shimadzu). The film thickness was measured by a profilometer (Altisurf 500, Altimet) using an inductive probe. Field-Emission Scanning Electron Microscopy (FESEM, JEOL) was employed to observe the morphology of the films. It was also equipped with an Energy Dispersive Spectrometer (EDS, Bruker) to analyze the chemical composition of the films.

### 2.3. Photocatalytic experiment

Regarding the photocatalytic activity experiment, a 150 W Xenon light source was used with a UV-400 cut-off filter to provide visible light. For a more intense illumination, a 400 W metal halide light source was also utilized to obtain higher photoactivity in an optimum situation. The sample (8 mm<sup>2</sup>/ml) was immersed in the Rhodamine-B (RhB) solution (5 mg/L) with a 15 cm distance from the light source and remained in the dark for 30 min before illumination to reach adsorption-desorption equilibrium, and then 2 mL

of the solution sample was retrieved every hour to analyze the concentration based on Beer-Lambert principle using a UV-Vis spectrophotometer (Libra). The pH of RhB solution was set to 3 using hydrochloric acid since the BiVO<sub>4</sub> thin films show the highest photoactivity at pH = 3 [23]. A blank test was performed to distinguish the effect of photolysis in the photodegradation process.

The photodegradation of organic pollutions follows pseudo-first-order kinetics through (eq. 1) [25].

$$\ln \frac{C_0}{C_t} = k't \quad (1)$$

Where  $t$  is the illumination time under the visible light,  $C_0$  is the initial concentration and  $C_t$  is the concentration at time  $t$ , and  $k'$  is the rate constant. Therefore, using this model, the kinetics of RhB photodegradation by BiVO<sub>4</sub> thin films were studied.

### 3. Results and discussion

The BiVO<sub>4</sub> thin film with a thickness of 932 nm deposited on fused silica was prepared using reactive DC magnetron sputtering after 180 min of deposition runtime. The EDS result related to the as-deposited thin film, shown in Fig. 1, proves that the films achieved the desired stoichiometric atomic composition, i.e., 1:1 for Bi:V in the deposition process. Since the EDS method does not provide an accurate estimation for oxygen, the metallic ratio of the elements was

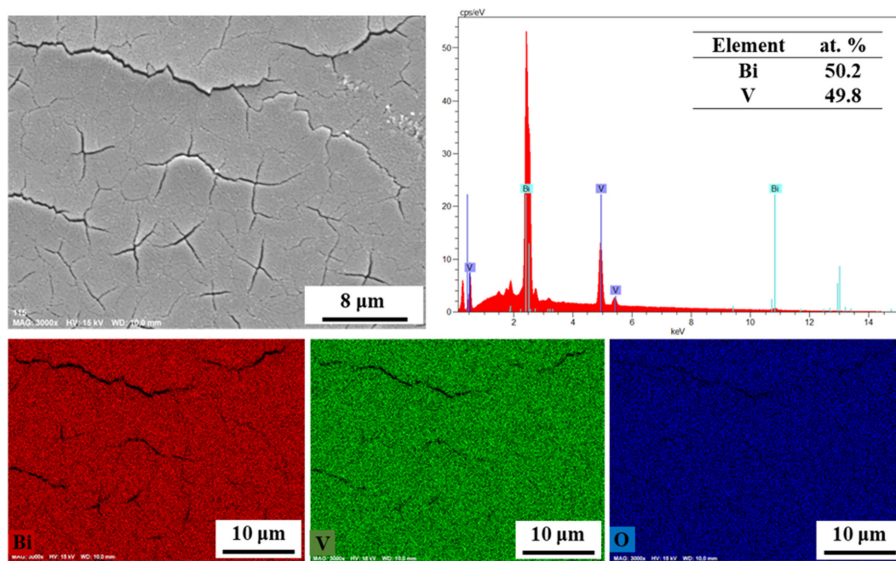


Fig. 1- FESEM mappings and EDS result of the BiVO<sub>4</sub> sample deposited on fused silica substrate and annealed at 450 °C under the air.

only considered here. The corresponding FESEM elemental mappings of the annealed sample at 450 °C demonstrate a proper atomic distribution of Bi, V and O elements throughout the surface shown by the red, green and blue colors, respectively. This shows the homogeneous deposition of the film in the sputtering process.

The XRD characterization was utilized to

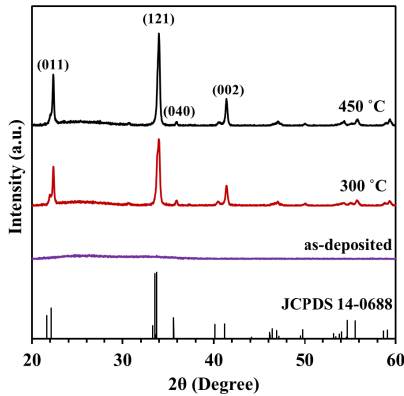


Fig. 2- XRD patterns of the  $\text{BiVO}_4$  samples deposited on fused silica substrate and annealed at different temperatures in air.

investigate the crystallographic structure of the thin films. As it can be seen in Fig. 2, the as-deposited sample is amorphous. Therefore, to achieve the monoclinic crystalline phase that is desired for photocatalytic activity, the sample underwent a post-annealing treatment for 2 h at 300 and 450 °C. While, at both temperatures, the desired crystalline phase was achieved (monoclinic scheelite structure, JCPDS No.14-0688), the average of crystallite size values showed slightly enhanced crystallinity towards the film annealed at 450 °C with a 48 nm crystallite size compared to 45 nm concerning the film annealed at 300 °C. The higher intensity of the peak concerning the (121) crystallographic plane at  $2\theta = 33.7^\circ$  verifies this statement. No secondary phase was detected in the XRD patterns.

The XPS technique was employed to evaluate the surface chemistry of the thin film annealed at 450 °C. The XPS results are provided in Fig. 3. The survey graph depicted in Fig. 3 (a) shows the existence of Bi, V, O and C elements, which are in agreement with the EDS results in Fig. 1. The peaks representing  $\text{Bi } 4f_{7/2}$  and  $\text{Bi } 4f_{5/2}$  at 159.3

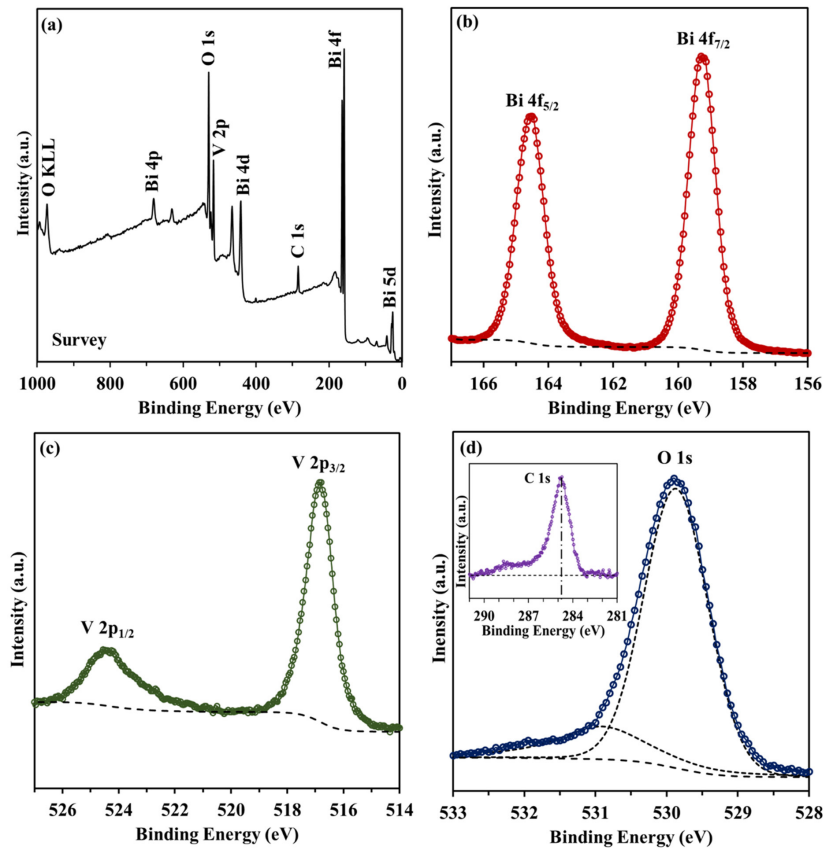


Fig. 3- XPS results of the thin film annealed at 450 °C, (a) survey, (b), (c) and (d) high-resolution spectra of Bi, V and O, respectively, and the inset graph is C 1s.

and 164.6 eV [26], respectively, are shown in Fig. 3 (b) proving the existence of Bi exclusively in Bi<sup>+3</sup> oxidation state. The two peaks at 516.8 and 524.3 eV, in Fig. 3 (c), represent V 2p<sub>3/2</sub> and V 2p<sub>1/2</sub> [27], respectively, belonging to the V<sup>+5</sup> oxidation state with no detection of V<sup>+4</sup> oxidation state. The peak related to O 1s depicted in Fig. 3 (d), was deconvoluted to the peaks at 529.9 and 530.9 eV, corresponding to lattice and adsorbed oxygen [28], respectively. The inset graph in Fig. 3 (d), shows the C 1s spectrum, due to carbon contamination, which is used to calibrate all the XPS spectra for charge correction.

The morphology of the thin films was observed by FESEM and the images are shown in Fig. 4. The as-deposited thin film, shown in Fig. 4 (a), demonstrates a uniform surface with no observable cracks and separate domains. Fig. 4 (b) shows that the film annealed at 300 °C consists of large cracks with an average size of approximately 2 μm. This could stem from the difference between the thermal expansion coefficient of the substrate (fused silica, 0.5 × 10<sup>-6</sup> C<sup>-1</sup>) and the film (BiVO<sub>4</sub>, 15.3 × 10<sup>-6</sup> C<sup>-1</sup>) [29], causing cracks due to stress relaxation. The top surface morphology of the film annealed at 450 °C is shown in Fig. 4 (c). The average crack size was slightly decreased, while nanometric pores formed on the surface in the shape of black dots in the range of 20–40 nm. The formation of nanopores has been observed in the case of low melting alloys after ion irradiation due to the

rise of temperature in local regions [30]. Herein, the Bi melting point is around 271 °C, while the annealing temperature concerning the thin film shown in Fig. 4 (c) is 450 °C. This results in the formation of local Bi molten areas, which then leads to the fast diffusion of V and O into these molten Bi through the interface of solid/liquid [31]. Therefore, this phenomenon results in the formation of the nanopores as a result of the coalescence of vacancies behaving according to the Kirkendall principle [32].

The influence of post-annealing treatment on the optical properties of the thin films was investigated using UV-Vis spectrophotometry and the results are shown in Fig. 5. The transmittance and reflectance of the as-deposited thin film along with the films annealed at 300 and 450 °C can be observed in Fig. 5 (a) and the inset graph. As the post-annealing temperature was raised, the transmission of light decreased, while the reflectance rose with more emphasis on the lower wavelength region. The absorbance, shown in Fig. 5 (b), was calculated using the (eq. 2) [19], and the bandgap was achieved using the Tauc plot given by (eq. 3) [19], and the results are shown in the inset graph Fig. 5 (b).

$$\alpha(\lambda) = \frac{1}{t} \ln \left( \frac{1 - R(\lambda)}{T(\lambda)} \right) \quad (2)$$

$$(\alpha h\nu)^{1/n} = A(h\nu - E_g) \quad (3)$$

Here, α(λ), R(λ), T(λ) are the absorption,

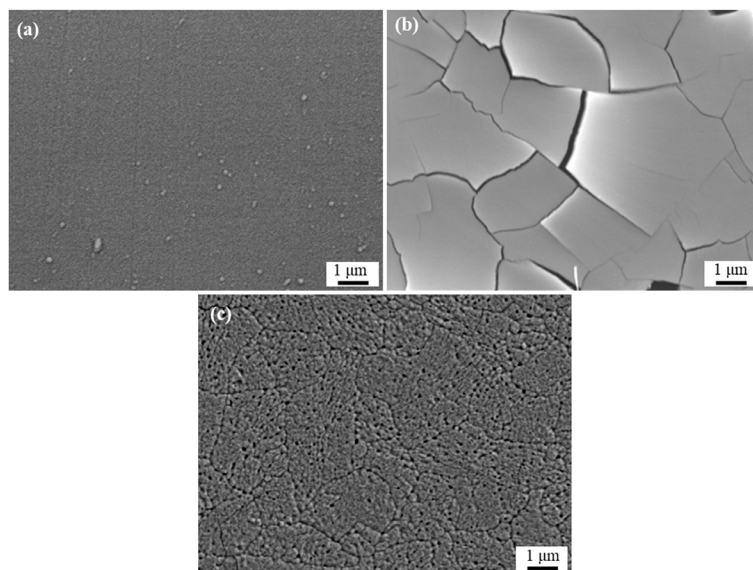


Fig. 4- FESEM images of the thin films (a) as-deposited, and annealed at (b) 300 and (c) 450 °C.

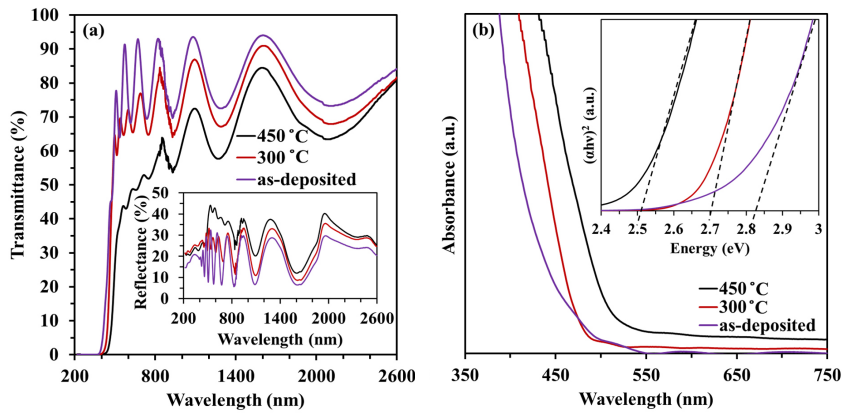


Fig. 5- (a) Transmittance and reflectance as inset, (b) absorbance and inset bandgap values of  $\text{BiVO}_4$  thin films annealed at different temperatures.

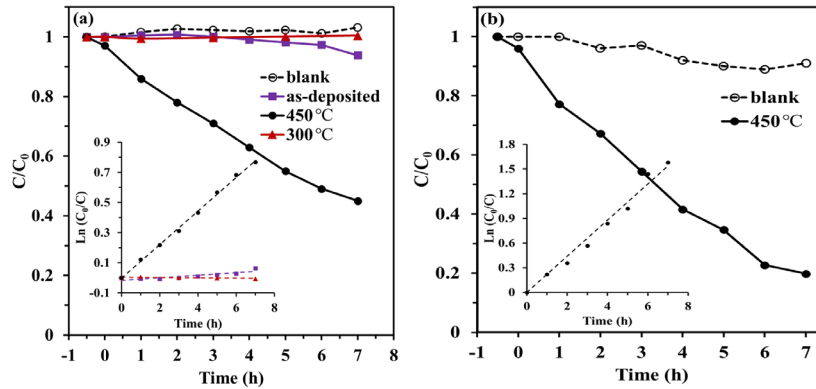


Fig. 6- (a) Photocatalytic experiment at pH = 3 by the as-deposited  $\text{BiVO}_4$  thin film and the films annealed at 300 and 450 °C using 150 W light source and (b) the photocatalytic activity of the optimum sample utilizing a 400 W light source. The inset graphs are pseudo-first-order kinetics of the photoreactions.

reflection and transmission coefficients, respectively, as a function of wavelength,  $t$  represents the film thickness,  $h$  is the Planck constant,  $\nu$  is the photon frequency,  $A$  is a constant, and  $E_g$  is the bandgap energy.  $n$  is set to 0.5, given  $\text{BiVO}_4$  is a direct bandgap semiconductor [33]. The thin film annealed at 450 °C, exhibits higher absorption of visible light photons with a bandgap of 2.5 eV, which agrees with the data published in the literature [26], while the values regarding the film annealed at 300 °C and the amorphous film are higher with 2.7 and 2.8 eV, respectively. This proves the visible light active characteristics of monoclinic  $\text{BiVO}_4$ . Meanwhile, it shows the effect of the nanoporous structure of the film in light absorption probably due to photon entrapment and light scattering inside the film.

The experiment of the photocatalytic degradation of RhB was conducted at pH = 3

to comparatively evaluate the post-annealing treatment effect on the photocatalytic performance of  $\text{BiVO}_4$  thin films, employing a 150 W Xenon light source and the results are illustrated in Fig. 6. The kinetics results are also provided in the inset graphs. It can be seen in Fig. 6 (a) that only the sample annealed at 450 °C showed photoactivity (55 % photodegradation of RhB after 7 h,  $k' = 0.11 \text{ h}^{-1}$ ), whereas other samples did not manage to photodegrade the RhB solution. This is probably due to superior light absorption and lower bandgap (2.5 eV) exhibited in Fig. 5, as well as the nanoporous morphology shown in Fig. 4 (c). The film with superior photoactivity was selected for an experiment in a more intense illumination to evaluate its performance in the optimum condition. Fig. 6 (b) demonstrates 80 % ( $k' = 0.22 \text{ h}^{-1}$ ) photodegradation of RhB solution. The 9 % decrease in the concentration concerning the blank test is the result of photolysis due to

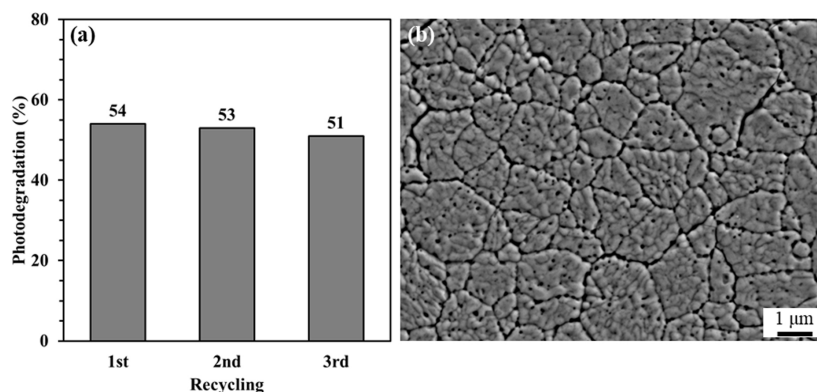


Fig. 7- (a) a 3-cycle (3 x 7 h exploitation) recycling experiment with a 150-W light source, (b) FESEM image of the sample after the experiment.

the intense illumination. These results show remarkable photoactivity of the  $\text{BiVO}_4$  thin film, produced by reactive DC magnetron sputtering.

The recycling test was performed to evaluate the stability of the nanoporous  $\text{BiVO}_4$  thin-film photocatalyst in the photodegradation of RhB in acidic conditions (pH = 3). Therefore, the experiment with three consecutive cycles (3 x 7 h of exploitation) was conducted under visible light provided by a 150 W Xe light source, and the results could be seen in Fig. 7. The photodegradation performance after three cycles shows a negligible decrease by only 3 %, illustrated in Fig. 7 (a), which is considered to be insignificant and therefore concludes a stable performance after 21 h of exploitation in acidic pH. While the FESEM image depicted in Fig. 7 (b) shows that slight corrosion of the grain boundaries might have happened due to the acidic condition at pH = 3, the microscopic integrity of the film is still completely intact, and no changes could be observed in the nanoporous morphology and pore sizes compared to the corresponding image related to the experiment before recycling shown in Fig. 4 (c). These results verify the stability of the  $\text{BiVO}_4$  thin films in the photocatalysis process for the wastewater treatment application.

#### 4. Conclusions

$\text{BiVO}_4$  thin-film photocatalysts were deposited on fused silica by reactive DC magnetron sputtering, and the photoactive monoclinic structure was achieved after a post-annealing treatment, which was verified by XRD.

XPS analysis verified the exclusive oxidation

states of  $\text{Bi}^{+3}$  and  $\text{V}^{+5}$ , as well as the existence of both lattice and adsorbed oxygen on the film surface.

The effect of post-annealing treatment on film properties was investigated by annealing the thin films at 300 and 450 °C. The film annealed at 450 °C had a nanoporous morphology unlike the one annealed at 300 °C. Raising the annealing temperature also decreased the bandgap values.

The highest photocatalytic activity was demonstrated by the thin film annealed at 450 °C with a nanoporous morphology, with the higher average of crystallite size (48 nm), lowest bandgap (2.5 eV) and highest visible light absorption.

The photocatalytic experiment showed a remarkable 80 % photodegradation of RhB solution ( $k' = 0.22 \text{ h}^{-1}$ ) after 7 h, and the recycling experiment proved the stability of the thin films after three consecutive cycles (21 h exploitation).

The results obtained in this research prove that nanoporous  $\text{BiVO}_4$  thin films prepared by the magnetron sputtering method could be good candidates for industrial and environmental wastewater treatment applications.

#### Conflict of interest

The authors declare that they have no conflict of interest.

#### Acknowledgments

The authors would like to acknowledge the supports of this study by the Iran National Science Foundation (project No: 98001285), Pays de Montbéliard Agglomération, and the Iran Nanotechnology Initiative Council for the support of this work.

## References

1. Tayebi M, Lee B-K. Recent advances in BiVO<sub>4</sub> semiconductor materials for hydrogen production using photoelectrochemical water splitting. *Renewable and Sustainable Energy Reviews*. 2019;111:332-43.
2. Peral J, Ollis D. Heterogeneous photocatalytic oxidation of gas-phase organics for air purification: Acetone, 1-butanol, butyraldehyde, formaldehyde, and m-xylene oxidation. *Journal of Catalysis*. 1992;136(2):554-65.
3. Behjati S, Sheibani S, Herritsch J, Gottfried JM. Photodegradation of dyes in batch and continuous reactors by Cu<sub>2</sub>O-CuO nano-photocatalyst on Cu foils prepared by chemical-thermal oxidation. *Materials Research Bulletin*. 2020;130:110920.
4. Razi R, Sheibani S. Photocatalytic activity enhancement by composition control of mechano-thermally synthesized BiVO<sub>4</sub>-Cu<sub>2</sub>O nanocomposite. *Ceramics International*. 2021;47(21):29795-806.
5. Yu C, Dong S, Zhao J, Han X, Wang J, Sun J. Preparation and characterization of sphere-shaped BiVO<sub>4</sub>/reduced graphene oxide photocatalyst for an augmented natural sunlight photocatalytic activity. *Journal of Alloys and Compounds*. 2016;677:219-27.
6. Holkar CR, Jadhav AJ, Pinjari DV, Mahamuni NM, Pandit AB. A critical review on textile wastewater treatments: Possible approaches. *Journal of Environmental Management*. 2016;182:351-66.
7. Chahkandi M, Zargazi M. New water based EPD thin BiVO<sub>4</sub> film: Effective photocatalytic degradation of Amoxicillin antibiotic. *Journal of Hazardous Materials*. 2020;389:121850.
8. Zhang X, Zhang Y, Quan X, Chen S. Preparation of Ag doped BiVO<sub>4</sub> film and its enhanced photoelectrocatalytic (PEC) ability of phenol degradation under visible light. *Journal of Hazardous Materials*. 2009;167(1-3):911-4.
9. Montakhab E, Rashchi F, Sheibani S. Effect of cathode size on the morphology of the anodized TiO<sub>2</sub> nanotube photocatalyst. *Journal of Ultrafine Grained and Nanostructured Materials*. 2021 Jun 20;54(1):85-92.
10. Fatolah M, Khayati GR. Facile decoration of CdS nanoparticles on TiO<sub>2</sub>: robust photocatalytic activity under LED illumination. *Zeitschrift für Naturforschung B*. 2021;0(0).
11. Paul KK, Giri PK. Plasmonic Metal and Semiconductor Nanoparticle Decorated TiO<sub>2</sub>-Based Photocatalysts for Solar Light Driven Photocatalysis. *Encyclopedia of Interfacial Chemistry*: Elsevier; 2018. p. 786-94.
12. Meng X, Zhang Z. Bismuth-based photocatalytic semiconductors: Introduction, challenges and possible approaches. *Journal of Molecular Catalysis A: Chemical*. 2016;423:533-49.
13. Gao X, Wang Z, Zhai X, Fu F, Li W. The synthesis of lanthanide doped BiVO<sub>4</sub> and its enhanced photocatalytic activity. *Journal of Molecular Liquids*. 2015;211:25-30.
14. Sharma R, Uma, Singh S, Verma A, Khanuja M. Visible light induced bactericidal and photocatalytic activity of hydrothermally synthesized BiVO<sub>4</sub> nano-octahedrals. *Journal of Photochemistry and Photobiology B: Biology*. 2016;162:266-72.
15. Wang M, Yang G-j, You M-y, Xie Y-h, Wang Y-z, Han J, et al. Effects of Ni doping contents on photocatalytic activity of B-BiVO<sub>4</sub> synthesized through sol-gel and impregnation two-step method. *Transactions of Nonferrous Metals Society of China*. 2017;27(9):2022-30.
16. Yu J, Zhang Y, Kudo A. Synthesis and photocatalytic performances of BiVO<sub>4</sub> by ammonia co-precipitation process. *Journal of Solid State Chemistry*. 2009;182(2):223-8.
17. Samsudin MFR, Sufian S, Hameed BH. Epigrammatic progress and perspective on the photocatalytic properties of BiVO<sub>4</sub>-based photocatalyst in photocatalytic water treatment technology: A review. *Journal of Molecular Liquids*. 2018;268:438-59.
18. Lu F, Chen K, Feng Q, Cai H, Ma D, Wang D, et al. Insight into the enhanced magnetic separation and photocatalytic activity of Sn-doped TiO<sub>2</sub> core-shell photocatalyst. *Journal of Environmental Chemical Engineering*. 2021;9(5):105840.
19. Sarkar S, Das NS, Chattopadhyay KK. Optical constants, dispersion energy parameters and dielectric properties of ultra-smooth nanocrystalline BiVO<sub>4</sub> thin films prepared by rf-magnetron sputtering. *Solid State Sciences*. 2014;33:58-66.
20. Ma C, Lee J, Kim Y, Cheol Seo W, Jung H, Yang W. Rational design of α-Fe<sub>2</sub>O<sub>3</sub> nanocubes supported BiVO<sub>4</sub> Z-scheme photocatalyst for photocatalytic degradation of antibiotic under visible light. *Journal of Colloid and Interface Science*. 2021;581:514-22.
21. Bakhtiarnia S, Sheibani S, Aubry E, Sun H, Briois P, Arab Pour Yazdi M. One-step preparation of Ag-incorporated BiVO<sub>4</sub> thin films: plasmon-heterostructure effect in photocatalytic activity enhancement. *Applied Surface Science*. 2022;580:152253.
22. Ullah H, Tahir AA, Mallick TK. Structural and electronic properties of oxygen defective and Se-doped p-type BiVO<sub>4</sub>(001) thin film for the applications of photocatalysis. *Applied Catalysis B: Environmental*. 2018;224:895-903.
23. Bakhtiarnia S, Sheibani S, Billard A, Sun H, Aubry E, Yazdi MAP. Enhanced photocatalytic activity of sputter-deposited nanoporous BiVO<sub>4</sub> thin films by controlling film thickness. *Journal of Alloys and Compounds*. 2021;879:160463.
24. Dong Q, Yang F, Liang F, Zhang Y, Xia D, Zhao W, et al. Silver particle on BiVO<sub>4</sub> nanosheet plasmonic photocatalyst with enhanced photocatalytic oxidation activity of sulfadiazine. *Journal of Molecular Liquids*. 2021;331:115751.
25. Kumar KV, Porkodi K, Rocha F. Langmuir-Hinshelwood kinetics – A theoretical study. *Catalysis Communications*. 2008;9(1):82-4.
26. Gao L, Long X, Wei S, Wang C, Wang T, Li F, et al. Facile growth of AgVO<sub>3</sub> nanoparticles on Mo-doped BiVO<sub>4</sub> film for enhanced photoelectrochemical water oxidation. *Chemical Engineering Journal*. 2019;378:122193.
27. Li M, Xu G, Guan Z, Wang Y, Yu H, Yu Y. Synthesis of Ag/BiVO<sub>4</sub>/rGO composite with enhanced photocatalytic degradation of triclosan. *Science of The Total Environment*. 2019;664:230-9.
28. Geng Y, Zhang P, Li N, Sun Z. Synthesis of Co doped BiVO<sub>4</sub> with enhanced visible-light photocatalytic activities. *Journal of Alloys and Compounds*. 2015;651:744-8.
29. Sinclair DC, Watson CJ, Howie RA, Skakle JMS, Coats AM, Kirk CA, et al. NaBi<sub>3</sub>V<sub>2</sub>O<sub>10</sub>: a new oxide ion conductor. *Journal of Materials Chemistry*. 1998;8(2):281-2.
30. Miyaji T, Nitta N. Nanoporous Structure Formation on the Surface of InSb by Ion Beam Irradiation. *Nanomaterials (Basel)*. 2017;7(8):204.
31. Cook GO, Sorensen CD. Overview of transient liquid phase and partial transient liquid phase bonding. *Journal of Materials Science*. 2011;46(16):5305-23.
32. Kim D, Chang J-h, Park J, Pak JJ. Formation and behavior of Kirkendall voids within intermetallic layers of solder joints. *Journal of Materials Science: Materials in Electronics*. 2011;22(7):703-16.
33. Walsh A, Yan Y, Huda MN, Al-Jassim MM, Wei S-H. Band Edge Electronic Structure of BiVO<sub>4</sub>: Elucidating the Role of the Bi s and V d Orbitals. *Chemistry of Materials*. 2009;21(3):547-51.